Micromagnetic analysis of injection locking in spin-transfer nano-oscillators

M. d'Aquino,[1] C. Serpico,[2] R. Bonin,[3] G. Bertotti,[4] and I. D. Mayergoyz[5]
[1]*Dipartimento per le Tecnologie, Università degli Studi di Napoli "Parthenope," I-80143 Napoli, Italy*
[2]*Dipartimento di Ingegneria Elettrica, Università di Napoli "Federico II," I-80125 Napoli, Italy*
[3]*Politecnico di Torino-Sede di Verrès, Verrès, I-11029 Aosta, Italy*
[4]*Istituto Nazionale di Ricerca Metrologica (INRiM), I-10135 Torino, Italy*
[5]*ECE Department and UMIACS, University of Maryland, College Park, Maryland 20742, USA*
(Received 18 May 2010; published 13 August 2010)

The injection-locking mechanism of a spin-transfer nano-oscillator is studied for a system which is traversed by a spin-polarized electric current with both dc and ac components. The uniform mode theory is used to predict the control parameters for the synchronization between the magnetization self-oscillation and the external microwave current. It is found that micromagnetic simulations at zero temperature are in very good agreement with the theory, showing that magnetization dynamics is practically uniform in space. Then, the effect of temperature on synchronized regimes is analyzed. The locking band as well as the hysteretic character of the oscillation response are determined as function of the control parameters. Computations of the power spectral densities (PSD) of injection-locked and unlocked oscillations reveal that synchronized oscillations are quite stable with respect to thermal fluctuations. Secondary peaks in the PSD of injection-locked oscillations are reported and theoretically explained.

DOI: 10.1103/PhysRevB.82.064415 PACS number(s): 05.45.Xt, 85.70.Kh, 75.40.Mg

I. INTRODUCTION

It has been shown, both theoretically and experimentally, that a spin-polarized electric current passing through a multilayer magnetic nanosystem can affect its magnetization state.[1,2] The interaction between spin-polarized current and magnetization in these nanosystems can produce large magnetization motions in far from equilibrium conditions. In particular, possible dynamical regimes under dc excitations include large-angle precessional magnetization dynamics. Spin transfer driven magnetization oscillations have very promising applications for the realization of current-controlled microwave oscillators integrable with semiconductor electronics.[3–10] This type of spin-transfer nano-oscillators (STNOs) could be used to realize a new design of clocks for synchronization of electronic devices.

For a single STNO, the microwave emitted power is very low and the self-oscillation frequency is not easily controllable, due to unavoidable tolerances in the fabrication of nanoscale devices. These limitations can be circumvented either by mutually synchronizing multiple STNOs[11,12] or by phase-locking magnetization oscillations to an external ac driving force,[13] for instance a microwave electric current or an external magnetic field at given frequency. The latter situation is often referred to as injection locking. In this way, a stable and sufficiently strong output signal with reduced linewidth can be obtained. Significant research efforts have been devoted to the theoretical study of mutual phase locking of multiple STNOs[14–16] and synchronization with external microwave sources.[17,18] Recent theoretical investigations[19,20] have pointed out that the phase-locking mechanism in large-angle magnetization oscillation regimes is tightly connected with the bifurcations of appropriate dynamical systems. One important consequence of the bifurcation analysis is that phase-locked magnetization oscillations exhibit hysteretic behavior[19,20] with respect to the spin-polarized current, which substantially deviates from standard phase-locking theory.[21,22]

In this paper we perform a micromagnetic analysis of current-driven injection-locking experiments for uniaxial trilayer magnetic nanosystems with out-of-plane tilted polarizer (see Fig. 1). We show that the spatially uniform mode theory is able to satisfactorily predict the control parameter space (dc current, ac current) for the observation of phase-locked oscillations. First, by using full micromagnetic simulations, it is shown that, under appropriate conditions, such oscillations are spatially uniform. Then, the influence of the thermal fluctuations on the synchronized regimes is studied. In particular, it is shown that the locking band is weakly influenced by the effect of temperature whereas the hysteretic nature of the synchronization is appreciably reduced at

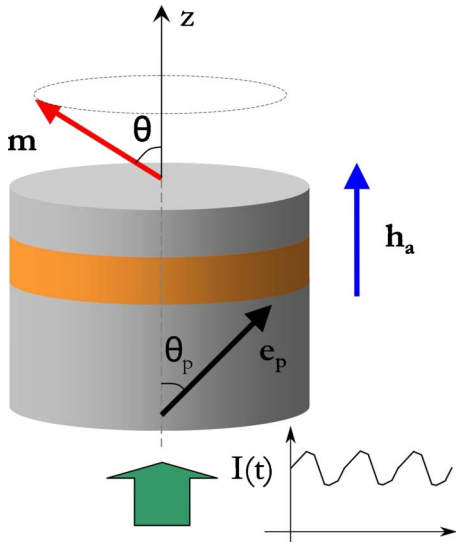

FIG. 1. (Color online) Sketch of a uniaxial trilayer spin valve.

room temperature. In addition, it is found that the power spectral density (PSD) of magnetization oscillations, computed for both phase-locked and unlocked regimes, reveals that the emitted microwave power and linewidth of the phase-locked oscillation are quite robust with respect to thermal fluctuations. It is pointed out that the PSD exhibits two secondary peaks symmetrically located around the central output frequency of the STNO. Such special feature of the PSD is explained by using the uniform mode theory, showing that the subpeaks are related to the linear response of an appropriate dynamical system.

The paper is organized as follows. In Sec. II, the fundamental equations which govern the dynamics of STNOs are introduced and the spatially uniform mode theory is developed. In Sec. III, the results of full micromagnetic simulations of a typical injection-locking experiment are reported and compared with the theory. In Sec. IV, the effects of thermal fluctuations on phase-locked magnetization oscillations are treated. First, the hysteretic nature of phase locking is analyzed when the system is at room temperature. Then, the power spectral densities of locked and unlocked oscillations are studied as function of temperature. In Sec. V, a comparison of the results of our analysis with the experimental data available in literature is reported. Finally, some conclusions and perspectives are presented in Sec. VI.

II. MODELLING ASPECTS

We consider a spin-valve trilayer structure with two (fixed and free) ferromagnetic layers separated by a conducting nonmagnetic spacer (see Fig. 1). The injected current $I(t)$ is composed of a dc component and a time-harmonic microwave component

$$I(t) = I_{\mathrm{dc}} + I_{\mathrm{ac}} \cos \omega t. \tag{1}$$

It is assumed that I_{dc} is sufficiently large to induce magnetization self-oscillations in the free layer and that ω is close to the self-oscillation frequency of the STNO. The external dc magnetic field is aligned with the z axis normal to the film plane and is assumed to be sufficiently strong that both the free and the fixed layer magnetization are tilted out of plane. The magnetization orientation of the fixed layer is assumed to be uniform. Spin-transfer oscillators subject to this kind of excitation conditions have been extensively studied experimentally.[23]

A. Fundamental equations

The magnetization dynamics in the free layer Ω is governed by the Landau-Lifshitz-Slonczewski equation, which can be written in normalized form as follows:[24]

$$\frac{\partial \mathbf{m}}{\partial t} = -\mathbf{m} \times \mathbf{h}_{\mathrm{eff}} - \alpha \mathbf{m} \times (\mathbf{m} \times \mathbf{h}_{\mathrm{eff}}) + \beta(t) \mathbf{m} \times (\mathbf{m} \times \mathbf{e}_p), \tag{2}$$

where $\mathbf{m}(\mathbf{r},t)$ is the unit vector describing the free layer magnetization (normalized by M_s) at each location $\mathbf{r} \in \Omega$, $\mathbf{h}_{\mathrm{eff}}[\mathbf{m}]$ is the effective field normalized by the free layer saturation magnetization M_s, time is measured in units of $(\gamma M_s)^{-1}$ (γ is the absolute value of the gyromagnetic ratio), and α is the damping constant. The vector field $\mathbf{m}$ satisfies the natural boundary condition $\partial \mathbf{m}/\partial \mathbf{n} = 0$ on the surface $\partial\Omega$. The micromagnetic effective field takes into account exchange, magnetostatics, anisotropy, and Zeeman interactions, and has the following expression:[24]

$$\mathbf{h}_{\mathrm{eff}}[\mathbf{m}] = \frac{l_{\mathrm{ex}}^2}{2} \nabla^2 \mathbf{m} + \mathbf{h}_m + \mathbf{h}_{\mathrm{an}} + \mathbf{h}_a, \tag{3}$$

where $l_{\mathrm{ex}} = \sqrt{2A/(\mu_0 M_s^2)}$ is the exchange length (A being the exchange constant of the material), $\mathbf{h}_m$ is the magnetostatic field produced by $\mathbf{m}$, $\mathbf{h}_{\mathrm{an}}$ is the anisotropy field and $\mathbf{h}_a$ is the external applied magnetic field.

The function $\beta(t)$ is proportional to $I(t)$ (positive when electrons flow from the free to the fixed layer) and measures the intensity of the spin-transfer effect while $\mathbf{e}_p$ is the unit vector in the direction of the fixed layer magnetization. In Eq. (2), for the sake of simplicity, we have neglected angular dependence of spin-transfer torque.[1]

The relationship between $I(t)$ and $\beta(t)$ is expressed as[25]

$$\beta(t) = b_p \frac{I(t)}{S J_p} = \frac{I(t)}{I_p}, \quad b_p = \frac{4P^{3/2}}{[3(1+P)^3 - 16P^{3/2}]}, \tag{4}$$

where S is the device cross sectional area, and $J_p = \mu_0 M_s^2 |e| d/\hbar$ is a characteristic current density (μ_0 is the vacuum permeability, e is the electron charge, d is the thickness of the free layer, and $\hbar$ is the reduced Planck constant). The parameter b_p depends on the polarization factor $0 < P < 1$ of the fixed layer.[1]

Since the current density $J_p \sim 10^9$ A cm^{-2}, one concludes that $\beta(t) \ll 1$ for typical experimental conditions. The function $\beta(t)$ is decomposed as follows:

$$\beta(t) = \beta_{\mathrm{dc}} + \beta_{\mathrm{ac}} \cos \omega t, \tag{5}$$

where $\beta_{\mathrm{dc}} = I_{\mathrm{dc}}/I_p$ and $\beta_{\mathrm{ac}} = I_{\mathrm{ac}}/I_p$. The smallness of $\beta(t)$ will be of special importance in the development of perturbation techniques.

B. Spatially-uniform mode theory

Analytical results for the injection-locking mechanism can be obtained under the assumption that the free layer magnetization is spatially uniform.[19]

Indeed, neglecting the spatial dependence of $\mathbf{m}$, Eq. (2) is reduced to the ordinary differential equation

$$\frac{d\mathbf{m}}{dt} = -\mathbf{m} \times \mathbf{h}_{\mathrm{eff}} - \alpha \mathbf{m} \times (\mathbf{m} \times \mathbf{h}_{\mathrm{eff}}) + \beta(t) \mathbf{m} \times (\mathbf{m} \times \mathbf{e}_p) \tag{6}$$

while the expression for the effective field [Eq. (3)] is appreciably simplified

$$\mathbf{h}_{\mathrm{eff}} = -D_x m_x \mathbf{e}_x - D_y m_y \mathbf{e}_y + (\mathrm{h}_{az} - D_z m_z) \mathbf{e}_z, \tag{7}$$

where h_{az} is the z component of the applied field and D_x, D_y, and D_z are the effective anisotropy constants taking into account shape and crystalline anisotropies.

It will be assumed that the polarizer unit-vector $\mathbf{e}_p$ is arbitrarily tilted out of plane

$$\mathbf{e}_p = \cos\ \theta_p \mathbf{e}_z + \sin\ \theta_p \mathbf{e}_x, \tag{8}$$

where θ_p is the angle between $\mathbf{e}_p$ and $\mathbf{e}_z$ (see Fig. 1).

It has been demonstrated[19] that the injection locking between self-oscillations of the system and the external microwave current can be studied by using suitable perturbation and averaging technique, based on the smallness of various parameters in the system. First, in typical experimental situations, the damping constant α is in the range 10^{-3}–10^{-2}. Then, as pointed out in the previous section, the normalized current $\beta(t)$ is a small quantity in Eq. (6). In fact, self-oscillations are excited when the spin-torque effect compensates dissipation,[25] namely, when β_{dc} is of the same order of smallness as α. In typical experimental conditions, the microwave component of the current is smaller than the dc component, meaning that $\beta_{\mathrm{ac}} < \beta_{\mathrm{dc}}$. We conclude that

$$\beta_{\mathrm{ac}}, \beta_{\mathrm{dc}} \sim \mathcal{O}(\alpha), \tag{9}$$

where the notation $\mathcal{O}(\alpha)$ means that the quantities are of the same order of smallness as α. We also assume that the free layer has weak in-plane crystalline anisotropy, which implies that $D_x, D_y \ll 1$. For this reason, the in-plane effective field $\mathbf{h}_{\mathrm{eff}\perp}$ is a small quantity as well

$$\mathbf{h}_{\mathrm{eff}\perp} = -D_x m_x \mathbf{e}_x - D_y m_y \mathbf{e}_y \sim \mathcal{O}(\alpha). \tag{10}$$

Equation (6) can be rewritten in perturbative form as follows:[19]

$$\frac{d\mathbf{m}}{dt} = \omega_0(m_z)\mathbf{e}_z \times \mathbf{m} + \mathbf{h}_{\mathrm{eff}\perp}(\mathbf{m}) \times \mathbf{m} - \alpha \mathbf{m} \times (\mathbf{m} \times \mathbf{h}_{\mathrm{eff}}) + \beta(t)\mathbf{m} \times (\mathbf{m} \times \mathbf{e}_p), \tag{11}$$

where

$$\omega_0(m_z) = h_{az} - D_z m_z. \tag{12}$$

Due to the smallness of α, $\beta(t)$, and $\mathbf{h}_{\mathrm{eff}\perp}$, the last three terms in the right-hand side of Eq. (11) are small quantities. For this reason, the differential equation containing only the first two terms can be interpreted as the unperturbed one and it describes precessional oscillations around the z axis with an angular frequency $\omega_0(m_z)$. From Eq. (11), one can conclude that there is a fast time scale related to the precessional motion, and a slow time scale associated with nonconservative effects (damping and spin-transfer torque).

The central idea developed in Ref. 19 is to derive an equation only describing the slow time scale dynamics in order to study the phase locking between the self-oscillations and the injected microwave current when the frequency ω is close to the natural frequency of the STNO. The derivation is based on observation that the vector $\beta(t)\mathbf{e}_p$ has a linearly polarized component $\beta_{\mathrm{ac}} \cos \omega t \mathbf{e}_p$. This component can be decomposed into two circularly polarized rotating vectors. Then, Eq. (11) can be rewritten in a reference frame rotating around the z axis at the angular speed ω with the same sense of rotation as the unperturbed precessional oscillations. In this new reference frame, the spin-torque term will have a constant component and one rotating with angular frequency -2ω. In order to obtain an autonomous equation, the right-hand side of the equation can be averaged over the period $T = 2\pi/\omega$, resulting in the following equation:[19]

$$\frac{d\mathbf{m}}{dt} = [\Omega_0(m_z) - \omega]\mathbf{e}_z \times \mathbf{m} - \alpha\left[\Omega_0(m_z) - \frac{\beta_z}{\alpha}\right]\mathbf{m} \times (\mathbf{m} \times \mathbf{e}_z) + \beta_a \mathbf{m} \times (\mathbf{m} \times \mathbf{e}_a), \tag{13}$$

where

$$\Omega_0(m_z) = h_{az} + \kappa_{\mathrm{eff}} m_z, \tag{14}$$

$$\kappa_{\mathrm{eff}} = -D_z + (D_x + D_y)/2, \tag{15}$$

$$\beta_a = (\beta_{\mathrm{ac}}/2)\sin\ \theta_p, \tag{16}$$

$$\beta_z = \beta_{\mathrm{dc}} \cos\ \theta_p. \tag{17}$$

It is important to stress that Eq. (13) describes an autonomous system evolving on the unit sphere $|\mathbf{m}| = 1$. As a consequence, the only steady-state solutions are either fixed points or limit cycles. Fixed points in the rotating reference frame represent periodic **P**-modes solutions in the laboratory frame while a limit cycle in the rotating frame produces a quasiperiodic **Q**-mode solution in the laboratory frame. Such quasiperiodic modes appear as a result of the combination of the periodic motion in the rotating frame and the uniform rotation with angular speed ω of the rotating frame. These mathematical facts can be used to study the injection-locking problem. Indeed, it is apparent that **P** modes correspond to phase-locked dynamical regimes for the magnetization of the free layer whereas **Q** modes indicate unlocked regimes.

It is worth to point out that, in order to have phase locking, it is necessary that both β_a and β_z must be nonzero. An immediate consequence of this observation is that the tilting angle θ_p of the polarizer magnetization is an essential factor of the locking mechanism. In fact, from Eqs. (16) and (17), it can be inferred that an in-plane polarizer, as well as a perpendicular one, could not lead to phase-locked regimes.

Moreover, for $\beta_a = \beta_{\mathrm{ac}} = 0$, Eq. (13) is formally identical to the equation for uniaxial spin-valve systems.[26] In this special situation, when $-1 \le (\beta_z/\alpha - h_{az})/\kappa_{\mathrm{eff}} \le 1$, Eq. (13) admits one limit cycle at a constant value of m_z given by the equation

$$\Omega_0(m_z) = \frac{\beta_z}{\alpha}, \quad m_z = \frac{\beta_z/\alpha - h_{az}}{\kappa_{\mathrm{eff}}}. \tag{18}$$

As it can be inferred from Eq. (13), in the laboratory frame this limit cycle consists of a precessional oscillation with frequency β_z/α. For this reason, the quantity β_z/α can be viewed as the "free running frequency" of the STNO before the ac current is injected. Therefore, the measure of the detuning of the ac current with respect to the oscillator frequency can be defined as

$$\Delta\omega = \frac{\beta_z}{\alpha} - \omega. \tag{19}$$

It is convenient to express Eq. (13) in spherical coordinates

$$\dot{\theta} = -\alpha[\Omega_0(\theta) - \beta_z/\alpha]\sin\ \theta - \beta_a \cos\ \theta \cos\ \phi, \tag{20}$$

$$\dot{\phi} = -[\Omega_0(\theta) - \omega] + (\beta_a/\sin\theta)\sin\phi. \tag{21}$$

In order to determine the **P** modes with coordinates (θ_0, ϕ_0), we have to find the stationary solutions of Eqs. (20) and (21), namely, imposing that $\dot{\theta}=0$ and $\dot{\phi}=0$. This leads to the following coupled equations:

$$\beta_a = [\Omega_0(\theta_0) - \omega]\sin\theta_0/\sin\phi_0, \tag{22}$$

$$\Delta\omega = [\Omega_0(\theta_0) - \omega](1 + \cot\phi_0 \cos\theta_0/\alpha), \tag{23}$$

which give the values of $\Delta\omega, \beta_a$ as function of (θ_0, ϕ_0) for given ω, h_{az}, κ_{eff}, and α.

The transition from locked **P**-mode regimes to unlocked regimes can be studied by analyzing the stability of the fixed points of the dynamical system [Eqs. (20) and (21)]. By linearizing the Eqs. (20) and (21) around a **P** mode and using standard stability analysis for two-dimensional dynamical systems,[19] in the limit of small detuning $\Delta\omega$, the bifurcation curve for the onset of locked regimes can be found on the control plane $(\Delta\omega, \beta_{\text{ac}})$ [or, equivalently using dimensional quantities $(\Delta f, I_{\text{ac}})$]

$$\beta_{\text{ac}} = \frac{2}{\sin\theta_p}\sqrt{\frac{1-[(\omega-h_{az})/\kappa_{\text{eff}}]^2}{1+[(\omega-h_{az})/\kappa_{\text{eff}}]^2/\alpha^2}}|\Delta\omega|. \tag{24}$$

The latter equation, along with Eqs. (17) and (19), allows one to estimate the dc current range for phase locking between the natural oscillations of the STNO and the injected microwave current, given the microwave current amplitude, the applied field h_{az}, the damping constant α and the frequency ω. In order to determine the locking range, one has to compute the bifurcation curves for limit cycles (**Q** modes) of the system defined by Eq. (20) and (21).

These two critical curves separate the control plane into the regions shown in Fig. 2. The region enclosed by the dashed lines, labelled as "P" includes the points $(\Delta f, I_{\text{ac}})$ where only phase-locked regimes exist. This implies that, for a given value of the ac current amplitude (see the horizontal line in Fig. 2), the segment CD defines the phase-locking band. Conversely, there exist two regions labelled as "Q" where only unlocked regimes can occur. Finally, there are two regions labelled as "P/Q" where either **P** or **Q** modes can occur. This means that the onset of a phase-locked oscillation regime depends on the history of the applied dc current. For example, if one starts with dc current at point A, the oscillation regime is unlocked. Then, if one increases the dc current, the magnetization oscillations will remain unlocked until the critical current value corresponding to point C is reached. Next, by further increasing the current, the system will be phase locked until point E is reached beyond which the **P** modes cannot exist. If one starts decreasing the dc current from point F, it is easy to see that the system will exhibit unlocked regimes until point D is reached, and the phase-locked oscillations will exist until the dc current is larger than that of point B. It is apparent that the outlined bifurcation mechanism gives rise to a hysteretic behavior of phase-locked magnetization oscillations.

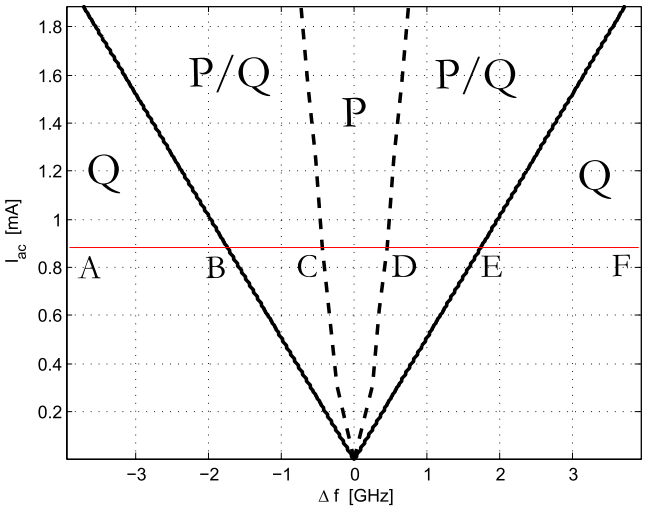

FIG. 2. (Color online) Bifurcation curves for onset of **P** modes and **Q** modes. Solid line refers to the bifurcation of **P** modes expressed by Eq. (24) while dashed line represents the bifurcation curve for **Q** modes, computed for the values of Table I and for $D_x=D_y=0.0344$, $D_z=0.9312$, $\kappa_{\text{eff}}=-0.8968$. The horizontal line refers to the ac current amplitude $I_{\text{ac}}=0.88$ mA used in the micromagnetic simulations. The points A, B, C, D, E, and F indicates the different current values in the various phases of the simulation.

III. FULL MICROMAGNETIC SIMULATIONS

In this section we study the phase locking for spin-transfer oscillators having typical structure and material parameters used in the experiments. We use the above theoretical predictions to estimate the parameters range suitable for observing synchronized regimes. Then, we perform full micromagnetic simulations of injection-locking experiments in order to check the applicability and accuracy of the theory.

To this end, we first define the parameters of the system under investigation. We consider an ultrathin disk with circular cross-section of diameter $D=135$ nm and thickness $d=3$ nm as free layer of the spin valve. The parameters of the permalloy free and fixed layer are: saturation polarization $J_s=\mu_0 M_s=1T$ (μ_0 is the vacuum permeability), exchange constant $A=1.3\times10^{-11}$ J/m, negligible anisotropy, damping constant $\alpha=0.02$ and polarization factor $P=0.3$. The tilting angle of the fixed layer is $\theta_p=45°$. The parameters used in the simulations are summarized in Table I.

The Landau-Lifshitz-Slonczewski [Eq. (2)] has been integrated by using a three-dimensional finite-difference micromagnetic numerical code based on the midpoint rule scheme.[27,28] The free layer is discretized by using 577 square prism cells with dimensions $5\times5\times3$ nm^3 (the mesh edge length is below the exchange length $l_{\text{ex}}=5.71$ nm).

We have simulated the following injection-locking experiment. The system is initially subject to the action of a strong external magnetic field $h_{az}\mathbf{e}_z$. Then, an electric current $I(t)$, with $I_{\text{dc}}=I_A=3.2$ mA and nonzero ac current I_{ac} at frequency $f=14$ GHz, is injected. Both dc and ac current amplitudes are kept constant for time intervals of about 60 ns, during which the system reaches a steady-state solution. Next, under constant ac amplitude, the dc current is slowly varied (in a

TABLE I. Parameters used in the simulations.

Geometrical parameters
Disk diameter $D=135$ nm
Disk thickness $d=3$ nm
Material parameters (Py)
Saturation magnetization $M_s=795.77$ kA/m ($\mu_0 M_s=1T$)
Exchange constant $A=1.3\times10^{-11}$ J/m
Exchange length $l_{ex}=5.71$ nm
Damping constant $\alpha=0.02$
Polarization factor $P=0.3$
Tilting angle of the polarizer $\theta_p=45°$ [see Eq. (8)]
References for dimensionless quantities
Frequency $f_0=\gamma M_s=175.87$ Ghz
Critical current density $J_p=3.62\times10^{12}$ A/m^2
$b_p=0.1659$ [see Eq. (4)]
Current $I_p=J_pS/b_p=312.52$ mA
Applied field and currents
External magnetic field $H_{az}=1.2M_s$
ac current $I_{ac}=0.88$ mA, frequency $f=14$ Ghz
dc current $I_A=3.2$ mA, $I_B=3.87$ mA, $I_C=4.28$ mA
dc current $I_D=4.56$ mA, $I_E=4.97$ mA, $I_F=5.6$ mA

time interval of 450 ns) in a linear fashion back and forth between the current values $I_{dc}=I_A=3.2$ mA ($\beta_{dc}=0.010$) and $I_{dc}=I_F=5.6$ mA ($\beta_{dc}=0.018$). This current interval includes the one computed by using the theoretical prediction given by Eq. (24) (the segment BE in Fig. 2), in order to check the hysteretic nature of the phase locking predicted by the uniform mode theory. The variation in I_{dc} vs time used in the simulations is shown in Fig. 3.

A. Spatial uniformity of magnetization

First, we have investigated the presence of spatial nonuniformities of the oscillations during the simulated experiment. To this end, in order to measure the degree of spatial nonuniformity of the magnetization dynamics, we have computed the quantity

$$u=\sqrt{1-(\langle m_x\rangle^2+\langle m_y\rangle^2+\langle m_z\rangle^2)}, \tag{25}$$

where the notation $\langle\cdot\rangle$ means spatial average over the free layer volume. The quantity [Eq. (25)] is able to reveal the onset of inhomogeneous magnetization ($u=0$ means spatial uniformity). The simulated injection-locking experiment has been repeated for three values of the ac current, namely, $I_{ac}=0.5, 0.88, 1.2$ mA.

The quantity u has been computed in the three cases and its temporal behavior is presented in Fig. 3. We have verified

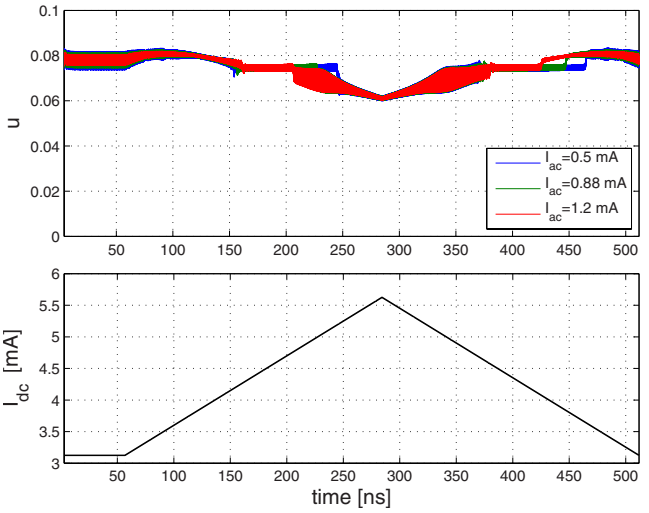

FIG. 3. (Color online) Top panel: magnetization spatial uniformity vs time computed according to Eq. (25) for $I_{ac}=0.5, 0.88, 1.2$ mA. Bottom panel: dc current I_{dc} vs time used in the simulations.

that it does not exceed 0.085 during the entire simulations, meaning that the magnetization is practically uniform.

B. Hysteresis in phase locking

The behavior of $\langle m_z\rangle$ component of the free layer magnetization as function of I_{dc} is reported in Fig. 4 (black lines). In order to make a comparison with the uniform mode theory, we have also computed $m_z=\cos\theta$ from numerical integration of the averaged Eqs. (20) and (21) (gray lines in Fig. 4). More precisely, the continuation of the solution $\theta(t)$ with respect to the parameter β_z has been performed for increasing and decreasing values of the dc current.

It is apparent that the micromagnetic simulations show the hysteretic nature of the phase-locking mechanism in very good agreement with the theoretical predictions of the uniform mode theory. It is worth to emphasize that this behavior is perfectly analogous to what happens for uniaxial STNOs subject to dc currents and radio-frequency applied fields.[20] Again, this means that bifurcation mechanisms play a fundamental role in the synchronization of large-angle magnetization oscillations with ac driving forces.

The power emitted by the STNO has been also studied by computing the spectrogram[29] of $\langle m_x\rangle(t)$ as function of the DC current for $I_{ac}=0.88$ mA. The results are shown in Fig. 5. One can clearly see that there are two large current intervals CE and DB in which magnetization oscillations are phase locked with the ac current at frequency $f=14$ GHz and the emitted power is maximum. The hysteretic nature of the phase-locking phenomenon is also evident from the spectrogram. Similar results (not reported for brevity) have been obtained for $I_{ac}=0.5, 1.2$ mA.

IV. EFFECT OF THERMAL FLUCTUATIONS IN PHASE LOCKING

In this section, we study the influence of temperature on the synchronization of the STNO with the external current. It

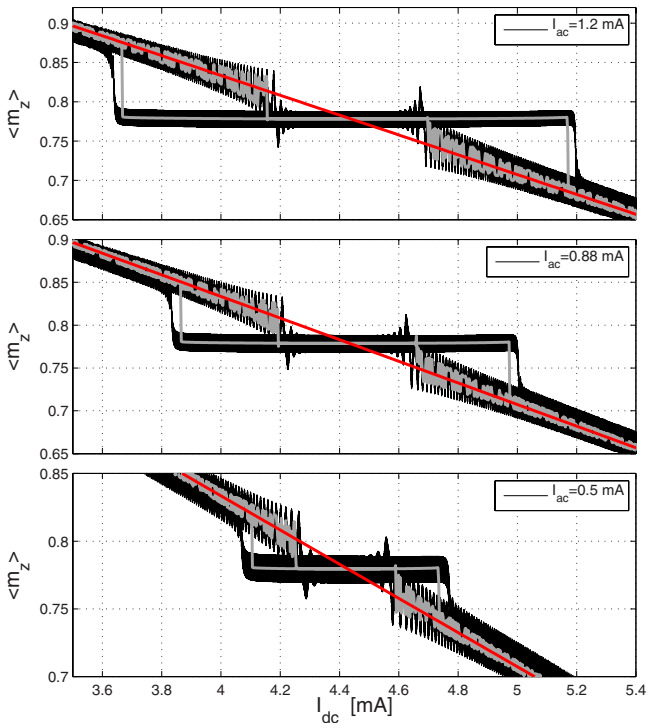

FIG. 4. (Color online) Magnetization response $\langle m_z \rangle$ as function of the dc current I_{dc}. Black solid lines are the result of micromagnetic simulation, the gray lines represent the theoretical predictions of Eqs. (20) and (21). The straight (red) lines refer to the m_z response, in the rotating frame, according to Eq. (18) in the absence of ac current.

is expected that the hysteretic behavior observed in zero-temperature simulations is appreciably reduced by the thermal fluctuations occurring at room temperature. This could explain why such hysteresis has not been observed so far in the experiments.[13,14]

In order to investigate this aspect, we note that, in the micromagnetic simulations described above, the magnetization has been almost uniform. This means that the actual magnetization dynamics can be well described by Eq. (6). In this situation, the presence of thermal fluctuations can be taken into account by augmenting the effective field $\mathbf{h}_{\mathrm{eff}}$ in Eq. (6) with an isotropic vector Gaussian white-noise thermal field $\mathbf{h}_{\mathrm{th}}$, leading to the following equation:[24]

$$\frac{d\mathbf{m}}{dt} = -\mathbf{m} \times (\mathbf{h}_{\mathrm{eff}} + \mathbf{h}_{\mathrm{th}}) - \alpha \mathbf{m} \times [\mathbf{m} \times (\mathbf{h}_{\mathrm{eff}} + \mathbf{h}_{\mathrm{th}})] + \beta(t)\mathbf{m} \times (\mathbf{m} \times \mathbf{e}_p). \tag{26}$$

In the latter equation, the variance ν^2 of the thermal field $\mathbf{h}_{\mathrm{th}}$ is derived by the fluctuation-dissipation[30] relation

$$\nu^2 = 2\alpha \frac{k_B T}{\mu_0 M_s^2 V}, \tag{27}$$

where T is the temperature, V is the volume of the free layer, and k_B is the Boltzmann constant.

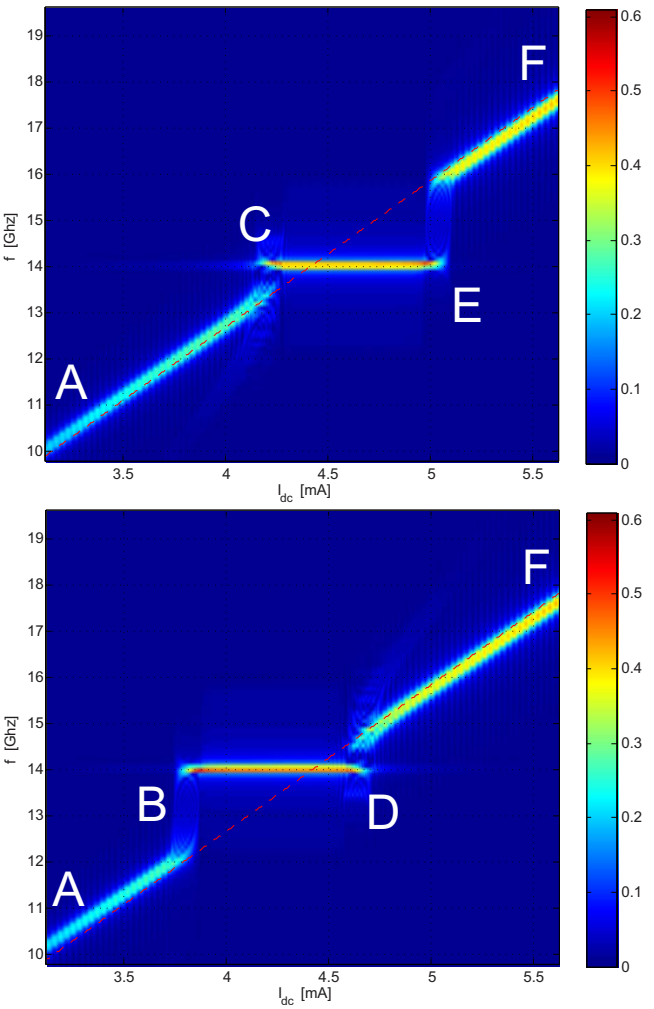

FIG. 5. (Color online) Spectrograms of $\langle m_x \rangle(t)$ for $I_{\mathrm{ac}} = 0.88$ mA. The upper plot is computed for I_{dc} increasing from I_A to I_F, the lower for I_{dc} decreasing from I_F to I_A. Dashed lines refer to the frequency response of the STNO for $I_{\mathrm{ac}}=0$ predicted by the uniform mode theory. Color plot refers to the amplitude of the in-plane magnetization oscillation $\langle m_x \rangle$.

We interpret Eq. (26) as stochastic differential equation in the sense of Stratonovich.[31] Magnetization $\mathbf{m}(t)$ becomes a stochastic process evolving on the unit sphere and its statistical properties can be derived by computing a sufficiently large number N of realizations of this stochastic process by direct numerical integration of Eq. (26). In order to preserve the conservation properties of stochastic magnetization dynamics, the implicit midpoint rule technique is adopted.[32] It is worth noting that the spatial uniformity of the dynamics demonstrated before makes the Langevin approach feasible since in the full micromagnetic framework,[33] it would require an enormous computational cost.

A. Temperature dependence of phase-locking hysteresis

First, we have numerically computed the critical curves for the bifurcations of **P** modes and **Q** modes at room temperature ($T=300$ K). Such critical curves have been obtained from the estimation of the ensemble average of $m_z(t)$

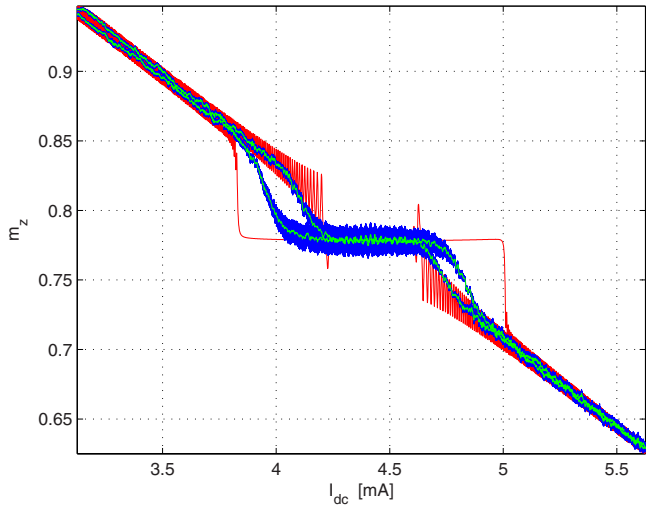

FIG. 6. (Color online) Magnetization response m_z vs dc current I_{dc} obtained by numerically integrating Eq. (26). The red line refers to results computed for $T=0$ K. The blue line refers to $\overline{m_z}$ computed by using $N=200$ realizations and $T=300$ K. The green line is a guide for the eyes obtained by averaging $\overline{m_z}(t)$ over time intervals equal to the period $1/f$ of the ac current.

$$\overline{m_z}(t) = \frac{1}{N}\sum_{k=1}^{N} m_{z,k}(t) \tag{28}$$

for $N=200$ realizations $m_{z,k}(t)$ of the magnetization stochastic process. An example of the computed $\overline{m_z}$ as function of I_{dc} is shown in Fig. 6.

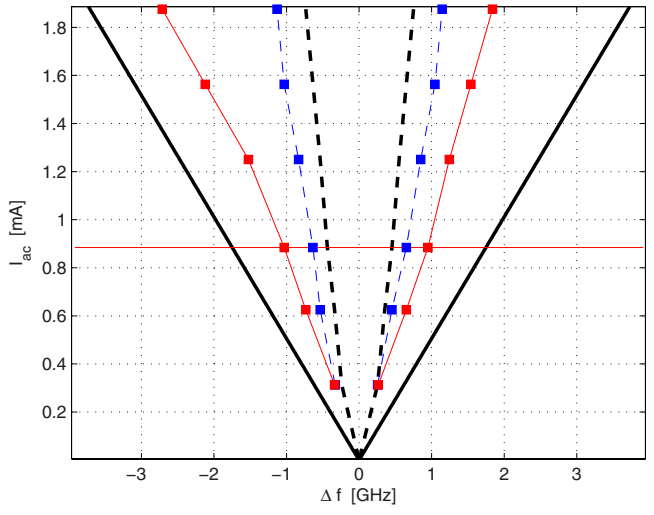

FIG. 7. (Color online) Critical curves for disappearance of **P** modes and **Q** modes. Solid line refers to the bifurcation of **P** modes expressed by Eq. (24) while dashed line represents the bifurcation curve for **Q** modes, computed for the values of Table I. The horizontal line refers to the ac current amplitude $I_{ac}=0.88$ mA used in the micromagnetic simulations. Solid red (dashed blue) lines with squares refer to bifurcation curves for **P** modes (**Q** modes) at room temperature $T=300$ K, computed using $N=200$ realizations of $m_z(t)$.

The critical bifurcation lines computed at $T=300$ K are presented in Fig. 7. One can observe that the thermal fluctuations strongly reduce the hysteretic behavior of synchronized regimes in comparison with deterministic dynamics, although it is still observable for microwave current amplitudes used in experiments.[13] On the other hand, the phase-locking band predicted by the deterministic theory (dashed bold line in Fig. 7) is slightly enlarged by thermal effects. This would suggest that synchronization by injection locking is quite robust with respect to temperature. Furthermore, from the spectrogram[29] shown in Fig. 8, it is clear that the microwave power emitted by the STNO when the oscillation is phase locked to the ac current is much higher than for unlocked regimes. Moreover, it is apparent from Fig. 8 that the oscillation linewidth is narrower in the phase-locking range.

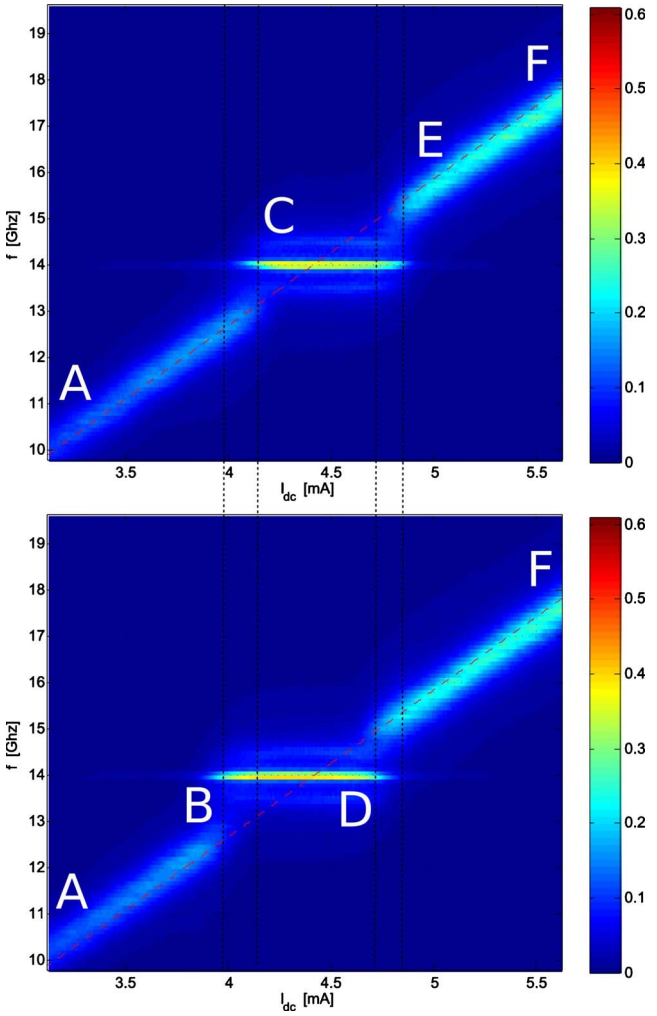

FIG. 8. (Color online) Spectrograms of $m_x(t)$ at $T=300$ K and $I_{ac}=0.88$ mA computed using $N=200$ realizations. The upper plot is computed for I_{dc} increasing from I_A to I_F, the lower for I_{dc} decreasing from I_F to I_A. Dashed lines refer to the frequency response of the STNO for $I_{ac}=0$ predicted by the uniform mode theory. Color plot refers to the amplitude of the in-plane magnetization oscillation m_x. Vertical dotted lines are guide for the eyes.

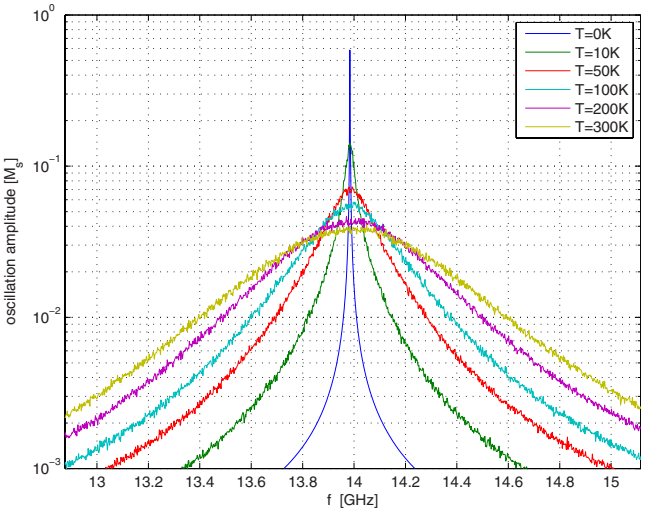

FIG. 9. (Color online) Power spectral density of $m_x(t)$ as function of temperature for $I_{dc}=4.42$ mA and $I_{ac}=0$ mA, numerically computed by averaging the spectra of $N=200$ realizations of $m_x(t)$.

B. Thermally induced sidebands in power spectral density of locked regimes

In order to compare phase-locked and unlocked magnetization oscillation regimes, we have computed the power spectral density[29] (PSD) of the in-plane magnetization component $m_x(t)$, for a given dc current $I_{dc}=4.42$ mA, with and without ac current. This value of I_{dc} is in the middle of the locking range, i.e., such that it yields zero detuning $\Delta f=0$ (see Fig. 7), and has been chosen in order to obtain a free running frequency of the STNO $f=14$ GHz, as it can be inferred from Eq. (18). The results, with and without injected ac current, are presented in Figs. 9–12. One can clearly see from Fig. 9 that, for $I_{ac}=0$ the oscillation linewidth becomes larger with increasing temperature while the quality factor of the oscillations is strongly reduced, whereas it remains almost constant when $I_{ac}=0.88$ mA (see Fig. 12). By looking at the oscillation amplitude in Fig. 10, it is also apparent that the phase-locked oscillations occur at large angle θ, which ensure a sufficiently strong signal detectable by GMR measurements. In addition, phase-locked oscillations exhibit a very narrow peak at the central frequency $f=14$ GHz (see Fig. 10), the full width half maximum (FWHM) linewidth is weakly dependent on temperature (see Fig. 11) and is in the order of few megahertz, which is comparable with observations in injection-locking experiments.[13,17] The results shown in Fig. 10 reveal another interesting feature of phase-locked magnetization oscillations. In fact, one can clearly see that, when thermal fluctuations are taken into account (even at very low temperatures), two secondary peaks appear in the PSD in symmetric position with respect to the central output frequency of the STNO. It is also worth noting that the frequencies corresponding to these subpeaks are almost independent of temperature.

Despite the strongly nonlinear nature of large-angle magnetization dynamics, this behavior presents the signature of linearity, as it can be well explained by using the theory discussed in Sec. II. In fact, as seen before, the phase-locked oscillations correspond to fixed points of the dynamical system [Eq. (13)] [or equivalently Eqs. (20) and (21)], which describes magnetization dynamics in the rotating frame. Let us now suppose that magnetization oscillation is phase locked to the injected ac current. This situation means that a well-defined stable **P** mode $s=(\theta_0,\phi_0)$ exists, which can be obtained from the solution of Eqs. (22) and (23) when the excitation conditions $(\Delta f, I_{ac})$ lie within the regions P and P/Q of Fig. 2. The corresponding portion of the phase portrait of the dynamical system defined by Eqs. (20) and (21) is depicted in Fig. 13, where one can clearly see that the fixed point s is a stable focus of the dynamics. When thermal fluctuations are present, the magnetization vector, considered in the rotating frame, is continuously 'kicked out' from the fixed point s (see Fig. 13). Moreover one can observe that, for the typical values of the parameters in Table I, the thermal field amplitude is a small quantity even at room temperature. Therefore, the stochastic dynamics of phase-locked oscillations can be reasonably described by a first-order perturbation of the system [Eqs. (20) and (21)] with respect to the **P** mode $s=(\theta_0,\phi_0)$. In other words, the system will relax to the equilibrium s with a linear damped response characterized by the complex-conjugate eigenfrequencies associated with the fixed point. Thus, by linearizing Eqs. (20) and (21) around the **P** mode (θ_0,ϕ_0), one can easily compute the frequency of the subpeaks by determining the eigenvalues of the matrix:

$$A_0 = \begin{bmatrix} -\alpha[\Omega_0(\theta_0)\cos\theta_0 - \kappa_{\text{eff}}\sin^2\theta_0 - \beta_z/\alpha\cos\theta_0] - \beta_a\sin\theta_0\cos\phi_0 & \beta_a\sin\phi_0 \\ \kappa_{\text{eff}}\sin\theta_0 - \beta_a\cos\theta_0/\sin^2\theta_0\sin\phi_0 & \beta_a/\sin\theta_0\cos\phi_0 \end{bmatrix}. \tag{29}$$

For our value of the control parameters $I_{dc}=4.42$ mA and $I_{ac}=0.88$ mA, the eigenvalues of A_0 are $\lambda_{1,2}=-0.0034\pm0.0233i$, which in physical units correspond to the frequency of ± 649 MHz and the linewidth of 190 MHz for each subpeak in the PSD. The oscillations characterized by these natural frequencies in the rotating frame, combined with the angular frequency of the rotating frame $f=14$ GHz, produce a PSD of $m_x(t)$ (in the lab frame) with two secondary peaks at frequencies 14 ± 0.649 GHz, each one having a FWHM linewidth of 190 MHz, which is in reasonable agreement with the results shown in Fig. 10. We have repeated these calculations for higher damping $\alpha=0.1$

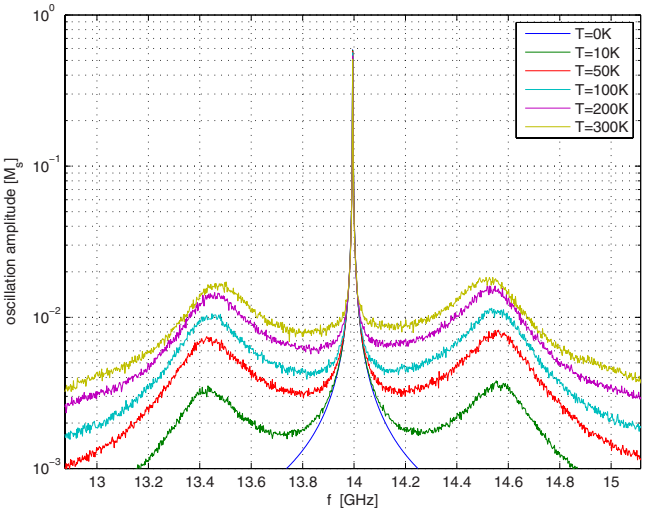

FIG. 10. (Color online) Power spectral density of $m_x(t)$ as function of temperature for I_{ac}=0.88 mA and I_{dc}=4.42 mA, numerically computed by averaging the spectra of N=200 realizations of $m_x(t)$.

and current amplitudes (not reported for sake of brevity) and verified that the theoretical predictions agree with the numerical results.

V. COMPARISON WITH EXPERIMENTS

It is instructive to compare our simulation results with available experimental data on injection locking of STNOs. The starting point for this comparison is the prediction of the control parameter space (dc and ac currents) for the observation of injection-locked oscillations. Our simulations reveal that the injection locking occurs when the dc current is in the range of 4–5 mA (see Figs. 4, 5, and 8) while the peak value of ac current is in the range of 0.5–1.2 mA. This compares well with the reported experimental results[13] where the injection locking was observed for the dc current of 7–8 mA and the peak value of ac current of 0.580 mA (0.410 mA rms). This agreement is quite satisfactory in view of existing design differences between STNOs used in experiments and numerical simulations.

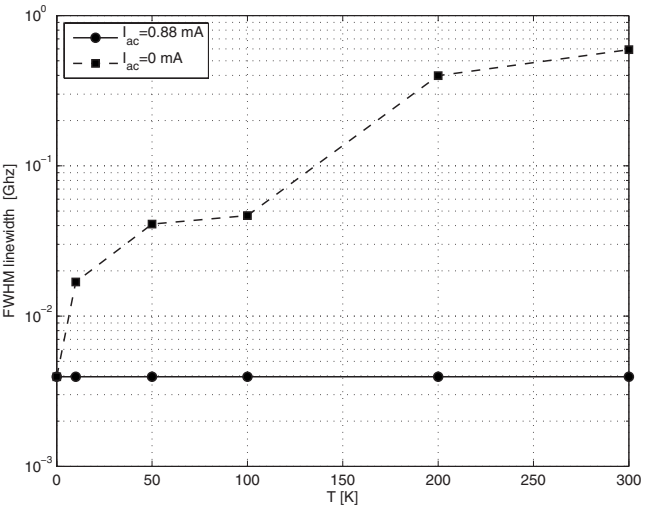

FIG. 11. FWHM linewidth as function of temperature for I_{dc} =4.42 mA, with I_{ac}=0.88 mA (solid line) and I_{ac}=0 mA (dashed line).

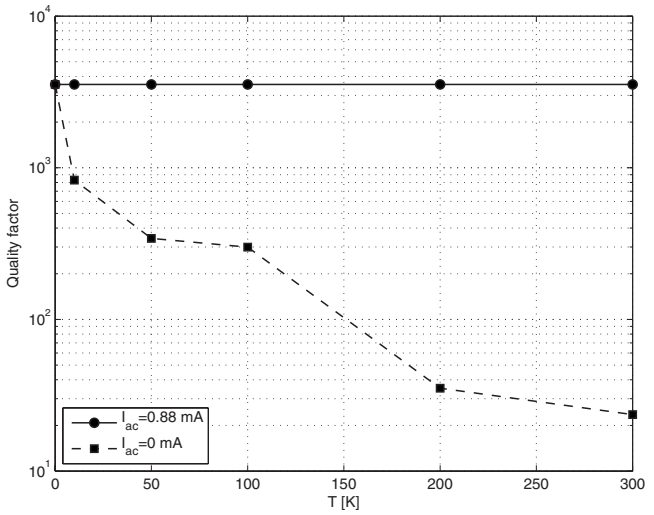

FIG. 12. Quality factor of the magnetization oscillation m_x as function of temperature for I_{dc}=4.42 mA, with I_{ac}=0.88 mA (solid line) and I_{ac}=0 mA (dashed line).

The presented micromagnetic simulations indicate that the spatial distribution of magnetization in the case of injection locking is quite uniform. There are no available data (to our knowledge) that explicitly reveal the spatial distribution of magnetization in injection-locking experiments. However, the fact that the linewidth of observed injection-locked oscil-

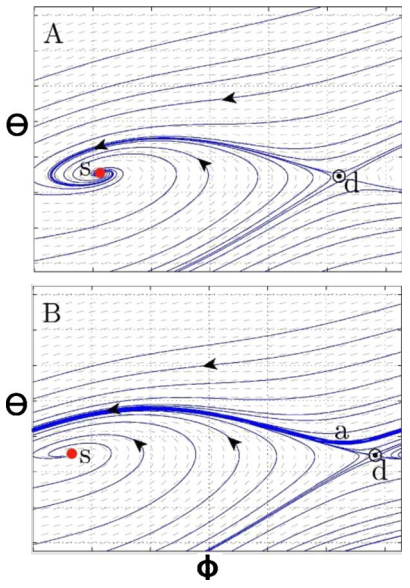

FIG. 13. (Color online) Qualitative representation of phase portrait of the dynamical system [Eqs. (20) and (21)] for excitation conditions $(\Delta f, I_{ac})$ in: (A) P regions; (B) P/Q regions of Fig. 2. In the diagrams, s represents a stable **P** mode (stable equilibrium), d is an unstable **P** mode (saddle point), and a is a stable **Q** mode (attracting limit cycle).

lations is quite narrow suggests that the spatial distribution of magnetization may be fairly uniform.

One of the main predictions of our theoretical and numerical analysis is the hysteresis phenomena in injection locking and its sensitivity to thermal fluctuations. As it is clear from Figs. 6 and 7, this thermal sensitivity may mask the hysteresis phenomena and make it difficult to detect. This may be the reason why the hysteresis in injection locking has not been observed experimentally until recently.[34] It has been reported[34] that at very low-temperature (5 K) hysteretic synchronization of STNOs has been observed and that hysteresis of injection locking is asymmetric with respect to the frequency detuning of the driving signals. This asymmetry at 0 K can be obtained if the asymmetric form of Sloncewski's torque[1] is used in the magnetization dynamics equation. Another reason for the asymmetry of hysteretic synchronization can be traced to thermal fluctuations. This is fully evident from Fig. 7 (see solid red lines with squares and dashed blue lines with squares).

Another important result of our simulations and theoretical analysis is the observation of secondary (side) peaks in the PSD of the output signal of STNOs. Similar side peaks in the PSD have been previously reported in the literature.[7] However, it seems to us that the presence of sidebands reported in the mentioned work is caused by the injection of an external ac modulation current at a relatively low frequency (40 MHz) as compared to the self-oscillation frequency (about 10 GHz). In contrast, it is demonstrated in the paper that the frequencies of side peaks of the PSD found in our simulations are due to thermally induced natural oscillations of magnetization around the phase-locked oscillations and these frequencies can be quantitatively determined by using the first-order perturbation technique.

VI. CONCLUSIONS

We have micromagnetically investigated current-driven injection-locking experiments for a uniaxial trilayer magnetic nanosystem with out-of-plane tilted polarizer. We have shown that the spatially uniform mode theory is able to satisfactorily predict the control parameter space (dc current, ac current) for the observation of phase-locked oscillations. Full micromagnetic simulations neglecting thermal effects have demonstrated that such oscillations are spatially quasiuniform. Then, the influence of the thermal fluctuations on the synchronized regimes has been studied. It has been shown that the locking band predicted by the theory is weakly enlarged by the effect of temperature whereas the hysteretic character of the synchronization is strongly reduced at room temperature. Nevertheless, from simulations it is expected that, with nanosystems having geometrical and material characteristics similar to those used in the paper, hysteresis might be observed in experiments at room temperature with microwave current amplitudes comparable with the ones reported in literature. In addition, analysis of the power spectral density PSD of the magnetization oscillation, computed for both phase-locked and unlocked regimes, shows that the emitted microwave power and the linewidth of the phase-locked oscillation are quite robust with respect to thermal fluctuations. Moreover, it has been pointed out that the PSD presents two secondary peaks symmetrically located around the central output frequency of the STNO, whose frequencies are almost independent on temperature. The characteristics of these secondary peaks have been explained and quantitatively determined by using a first-order perturbation technique in the spatially uniform mode theory, leading to a good agreement with the simulations. It is expected that these results might stimulate further experimental studies and discussions on injection-locking experiments and synchronization mechanisms of spin-transfer nano-oscillators.

[1] J. C. Slonczewski, J. Magn. Magn. Mater. **159**, L1 (1996).
[2] L. Berger, Phys. Rev. B **54**, 9353 (1996).
[3] W. Weber, S. Riesen, and H. C. Siegmann, Science **291**, 1015 (2001).
[4] S. I. Kiselev, J. C. Sankey, I. N. Krivorotov, N. C. Emley, R. J. Schoelkopf, R. A. Buhrman, and D. C. Ralph, Nature (London) **425**, 380 (2003).
[5] W. H. Rippard, M. R. Pufall, S. Kaka, S. E. Russek, and T. J. Silva, Phys. Rev. Lett. **92**, 027201 (2004).
[6] H. Xi, K. Gao, and Y. Shi, Appl. Phys. Lett. **84**, 4977 (2004).
[7] M. R. Pufall, W. H. Rippard, S. Kaka, T. J. Silva, and S. E. Russek, Appl. Phys. Lett. **86**, 082506 (2005).
[8] M. Tsoi, A. G. M. Jansen, J. Bass, W.-C. Chiang, M. Seck, V. Tsoi, and P. Wyder, Phys. Rev. Lett. **80**, 4281 (1998).
[9] J. Z. Sun, J. Magn. Magn. Mater. **202**, 157 (1999).
[10] M. Tsoi, A. G. M. Jansen, J. Bass, W.-C. Chiang, V. Tsoi, and P. Wyder, Nature (London) **406**, 46 (2000).
[11] S. Kaka, M. R. Pufall1, W. H. Rippard, T. J. Silva, S. E. Russek, J. A. Katine, Nature (London) **437**, 389 (2005).
[12] F. B. Mancoff, N. D. Rizzo, B. N. Engel, and S. Tehrani, Nature (London) **437**, 393 (2005).
[13] W. H. Rippard, M. R. Pufall, S. Kaka, T. J. Silva, S. E. Russek, and J. A. Katine, Phys. Rev. Lett. **95**, 067203 (2005).
[14] J. Grollier, V. Cros, and A. Fert, Phys. Rev. B **73**, 060409(R) (2006).
[15] A. N. Slavin and V. S. Tiberkevich, Phys. Rev. B **72**, 092407 (2005).
[16] A. N. Slavin and V. S. Tiberkevich, Phys. Rev. B **74**, 104401 (2006).
[17] B. Georges, J. Grollier, M. Darques, V. Cros, C. Deranlot, B. Marcilhac, G. Faini, and A. Fert, Phys. Rev. Lett. **101**, 017201 (2008).
[18] Z. Li, Y. C. Li, and S. Zhang, Phys. Rev. B **74**, 054417 (2006).
[19] C. Serpico, R. Bonin, G. Bertotti, M. d'Aquino, and I. D. Mayergoyz, IEEE Trans. Magn. **45**, 3441 (2009).
[20] R. Bonin, G. Bertotti, C. Serpico, I. D. Mayergoyz, and M. d'Aquino, Eur. Phys. J. B **68**, 221 (2009).
[21] R. Adler, Proc. IEEE **61**, 1380 (1973).
[22] A. N. Slavin, V. Tiberkevich, IEEE Trans. Magn. **45**, 1875 (2009).

[23] J. C. Sankey, P. M. Braganca, A. G. F. Garcia, I. N. Krivorotov, R. A. Buhrman, and D. C. Ralph, Phys. Rev. Lett. **96**, 227601 (2006).
[24] G. Bertotti, I. D. Mayergoyz, and C. Serpico, *Nonlinear Magnetization Dynamics in Nanosystems* (Elsevier, New York, 2009).
[25] G. Bertotti, C. Serpico, I. D. Mayergoyz, A. Magni, M. d'Aquino, and R. Bonin, Phys. Rev. Lett. **94**, 127206 (2005).
[26] Ya. B. Bazaliy, B. A. Jones, and S.-C. Zhang, Phys. Rev. B **69**, 094421 (2004).
[27] C. Serpico, I. D. Mayergoyz, and G. Bertotti, J. Appl. Phys. **89**, 6991 (2001).
[28] M. d'Aquino, C. Serpico, and G. Miano, J. Comput. Phys. **209**, 730 (2005).
[29] A. Papoulis, *Probability, Random Variables, and Stochastic Processes*, 3rd ed. (McGraw-Hill, New York, 1991).
[30] W. F. Brown, Phys. Rev. **130**, 1677 (1963).
[31] C. W. Gardiner, *Handbook of Stochastic Methods*, 2nd ed. (Springer, New York, 1997).
[32] M. d'Aquino, C. Serpico, G. Coppola, I. D. Mayergoyz, and G. Bertotti, J. Appl. Phys. **99**, 08B905 (2006).
[33] C. Ragusa, M. d'Aquino, C. Serpico, B. Xie, M. Repetto, G. Bertotti, and D. Ansalone, IEEE Trans. Magn. **45**, 3919 (2009).
[34] P. Tabor, V. Tiberkevich, A. Slavin, and S. Urazhdin, Phys. Rev. B **82**, 020407(2010).